



Targeting central nervous system extracellular vesicles enhanced triiodothyronine remyelination effect on experimental autoimmune encephalomyelitis

Yun Xiao^{a,1}, Jing Tian^{a,1}, Wen-Cheng Wu^{a,1}, Yu-Han Gao^a, Yu-Xin Guo^a, Sheng-Jiao Song^a, Rui Gao^a, Li-Bin Wang^b, Xiao-Yu Wu^b, Yuan Zhang^{a,*}, Xing Li^{a,**}

^a National Engineering Laboratory for Resource Development of Endangered Crude Drugs in Northwest China, The Key Laboratory of Medicinal Resources and Natural Pharmaceutical Chemistry, The Ministry of Education, College of Life Sciences, Shaanxi Normal University, Xi'an, Shaanxi, 710119, China

^b The General Hospital of Ningxia Medical University, Yinchuan, 750001, China

ARTICLE INFO

Keywords:

Extracellular vesicles
Neuroinflammation
Multiple sclerosis
Drug delivery
Experimental autoimmune encephalomyelitis
T3

ABSTRACT

The lack of targeted and high-efficiency drug delivery to the central nervous system (CNS) nidus is the main problem in the treatment of demyelinating disease. Extracellular vesicles (EVs) possess great promise as a drug delivery vector given their advanced features. However, clinical applications are limited because of their inadequate targeting ability and the “dilution effects” after systemic administration. Neural stem cells (NSCs) supply a plentiful source of EVs on account of their extraordinary capacity for self-renewal. Here, we have developed a novel therapeutic system using EVs from modified NSCs with high expressed ligand PDGF-A (EVPs) and achieve local delivery. It has been demonstrated that EVPs greatly enhance the target capability on oligodendrocyte lineage. Moreover, EVPs are used for embedding triiodothyronine (T3), a thyroid hormone that is critical for oligodendrocyte development but has serious side effects when systemically administered. Our results demonstrated that systemic injection of EVPs + T3, versus EVPs or T3 administration individually, markedly alleviated disease development, enhanced oligodendrocyte survival, inhibited myelin damage, and promoted myelin regeneration in the lesions of experimental autoimmune encephalomyelitis mice. Taken together, our findings showed that engineered EVPs possess a remarkable CNS lesion targeting potential that offers a potent therapeutic strategy for CNS demyelinating diseases as well as neuroinflammation.

1. Introduction

Oligodendrocytes (OLGs) are the myelinating cells of the central nervous system (CNS). They derive from oligodendrocyte progenitor cells (OPCs), which can differentiate into either astrocytes or OLGs depending on the microenvironment [1]. OLGs are myelin production cells that form the myelin sheath around axons and facilitate efficient signal transduction. However, OLGs are highly susceptible to damage because of the elevated metabolic rate and ATP requirement for the synthesis of myelin proteins [2]. Thus, the differentiation of OLGs from OPCs is critical for remyelination [3].

In demyelinating diseases, such as multiple sclerosis, endogenous

remyelination usually fails. This is due to the loss of trophic support for oligodendrocytes and accumulation of CNS regeneration inhibitors such as Nogo-A, myelin-associated glycoprotein (MAG), and oligodendrocyte myelin glycoprotein (OMgp) [4]. Thus, a focus on oligodendrogenesis is vital for developing effective strategies for myelin regeneration.

Adults with impaired thyroid hormone (TH) signaling are susceptible to demyelinating diseases such as multiple sclerosis (MS) [5]. It is not surprising that triiodothyronine (T3), a thyroid hormone that affects various physiological processes, promotes OLG differentiation via regulation of myelin genes such as myelin basic protein (MBP), proteolipid protein (PLP), and 2',3'-cyclic nucleotide 3' phosphodiesterase (CNPase) [6]. Mechanically, in the presence of T3, both thyroid

Peer review under responsibility of KeAi Communications Co., Ltd.

* Corresponding author.

** Corresponding author.

E-mail addresses: yuanzhang_bio@126.com (Y. Zhang), xingli_xian@126.com (X. Li).

¹ These authors contributed equally to this work.

<https://doi.org/10.1016/j.bioactmat.2021.07.017>

Received 10 November 2020; Received in revised form 24 June 2021; Accepted 19 July 2021

Available online 24 July 2021

2452-199X/© 2021 The Authors. Publishing services by Elsevier B.V. on behalf of KeAi Communications Co. Ltd. This is an open access article under the CC

BY-NC-ND license (<http://creativecommons.org/licenses/by-nc-nd/4.0/>).

hormone receptor alpha (TR α) and TR β specifically bind to the promoter region of the MBP within the TREs [7]. Although T3 is trophic during OLG development, the import of T3 in these cells is limited by the capacity of monocarboxylate transporter 8 (MCT8), a specific TH transporter [8]. In addition, the intracellular level of T3 is controlled by deiodinases [9]. Specifically, in the disease state, the activity of Dio3 increases to convert excess T3 into diiodothyronine (T2) and prevent the further generation of T3 [5]. Even though T3 may promote myelin regeneration in the CNS, excessive administration of THs may cause local hyperthyroidism in the immune organs. Administration of T3 also induces a peripheral immune reaction, which increases side effects and harm to the tissue. Therefore, innovative targeted nanoparticle-loaded T3 will be promising for better CNS drug delivery.

Extracellular vesicles (EVs) are membrane-bound organelles released by all cells and tissue types [10]. Owing to containing various types of molecular cargo, such as enzymes, receptors, mRNA, microRNA, and metabolites [11,12], EVs have recently gained significant attention as potential drug carriers, disease biomarkers, and important mediators of intercellular communication for different purposes (e.g., inflammation, cancer). In general, the size of EVs ranges from 10 to 1000 nm, and EVs can be subdivided into different types, including exosomes (<150 nm) and microvesicles (\leq 1000 nm) [12]. It has been reported that EVs were used for the delivery of small molecules and nucleic acids and showed promise in the clinical therapeutic field [12]. However, systemically delivered EVs accumulate in the liver and spleen [13]. Approaches of modifying EVs to target specific cell types would enhance their therapeutic potential [14].

There are multiple advantages of EVs compared to manufactured drug vehicles, such as liposomes or nanomaterials. First, EVs directly fuse with the target cell plasma membrane and do not need post-fabrication modifications [11,15]. Second, EVs can be acquired from patients' cells, and they lack immunogenic than synthetic delivery carriers. Last but not least, the naturally small size of EVs is able to cross the blood–brain barrier (BBB), spread to the cerebrospinal fluid, and reach distant tissues easily [16,17]. These promising benefits of EVs for therapeutic applications in disease make them ideal carriers for drug delivery.

Here, we report that EVs derived from NSCs expressing the ligand of PDGF-A (EVPs) and injected by intravenous during the peak of EAE dramatically increase targeting efficiency to the lineage of OLGs in the CNS. In addition, these EVPs loaded with low dosages of T3 (EVPs-T3) have the therapeutic ability to significantly suppress the disease development in the lesion and protect against myelin loss. Further, immunofluorescence results showed that EVPs-T3 remarkably increases the number of APC⁺ mature OLGs in the lesion. Electron microscope data indicated that EVPs-T3 dramatically promote myelin regeneration *in vivo*. These engineered EVPs represent an impactful tool for further application of EVs in the treatment of CNS disease.

2. Material and methods

2.1. EV isolation

EVs were extracted from the supernatant of neural stem cells. Before harvesting the cell culture medium, NSCs [4] were digested by Accutase (Thermo Fisher Scientific, Waltham, USA), and the cultured medium contained DMEM/F12 combined with a B27 supplement (Thermo Fisher Scientific). For 2 days of culturing, the EVs were isolated from the medium by ultracentrifugation. Briefly, the cell culture medium was centrifuged at 300 \times g for 10 min to discard cells, 1200 \times g for 20 min, and 8000 \times g for half an hour to cast away extra cell debris at the tube bottom. Finally, the medium was filtered with a 0.22 μ m filter (Millipore, Billerica, USA) and centrifuged at 110,000 \times g for 70 min at 4 °C in an SW 40 Ti rotor using an Optima XPN-100 ultracentrifuge (Beckman Coulter, Brea, USA) to harvest the EVs. The supernatant was removed carefully, and the EVs were washed with PBS, ultracentrifuged again, and were

precipitated at bottom of the tube.

2.2. Vector construct and lentivirus package

The primers of PDGFA were synthesized by the Beijing Genomics Institute (Beijing, China), and the nucleotide sequences are listed in [Supplementary Table 1](#). The C1C2 domain of MFG-E8 was inserted into the vector of Lenti-XStamp, which was purchased from System Biosciences (Palo Alto, USA), was inserted into the vector of Lenti-XStamp. The fragment of PDGFA was inserted into the Lenti-XStamp, and the lentivirus was packaged following the instruction of the pPACKH1 HIV Lentivector Packaging Kit (System Biosciences).

2.3. Cell culture

NSCs were obtained following a previously described method [4] and plated in DMEM/F12 with B27 (Thermo Fisher Scientific), recombinant murine epidermal growth factor (rmEGF, 20 ng/ml), recombinant murine fibroblast growth factor (rmFGF, 10 ng/ml) (PeproTech, Rocky Hill, USA), penicillin, streptomycin (100 U/ml), and 2 mM L-glutamine.

To establish stable expression of PDGF on the surface of vesicles, we transduced the Lenti-XStamp-PDGFA virus into the NSCs. Since XStamp lentivector has a downstream neomycin element, it can be used for selection and stable cell line development. Neomycin (500 μ g/ml) was used to select the positive cells.

2.4. EV labeling

An EV Labeling Kit (System Biosciences) was used to mark the EVs, and the process followed the instructions. Briefly, the 6 μ l reaction buffer and 1 μ l labeling dye were mixed with EVs in the appropriate amount and incubated for half an hour at 25 °C. The free unlabeled dye was then removed by PD SpinTrap G-25 (GE, Buckinghamshire, UK), and the labeled EVs were used for a subsequent experiment.

2.5. Cell viability assay

OPCs were plated in a 96-well plate at 1.5×10^4 /ml for 24 h in 37 °C. The medium was then removed and replaced with 100 μ l of fresh culture medium containing CCK8 (TargetMol, USA). After 30 min, 1 h, 2 h, and 4 h, the absorbance at 450 nm was tested by the microplate reader.

2.6. OPC isolation

OPCs were dissected from the neonatal brain (animal age \leq P7). First, we used Neural Tissue Dissociation Kits (Miltenyi Biotec, Germany) to obtain single-cell suspensions. Then we used the CD140a (PDGF α) MicroBead Kit (Miltenyi Biotec, Germany) to label CD140a (PDGF α)⁺ cells. Finally, we obtained OPCs through LS columns (Miltenyi Biotec, Germany).

2.7. Branch score

Concentric circles separated by 15 μ m were drawn around the cell bodies of the microphotographed oligodendrocytes. The number of intersections that the oligodendrocyte processes made with the concentric circles was defined as the branching score using the Sholl analysis plugin for ImageJ software [18].

2.8. EAE

Female C57BL/6 mice, eight weeks of age, were obtained from the Fourth Military University (Xi'an, China). All experimental procedures and protocols were approved by the Animal Ethics Experimental Committee of Shaanxi Normal University. The EAE induction, clinical score

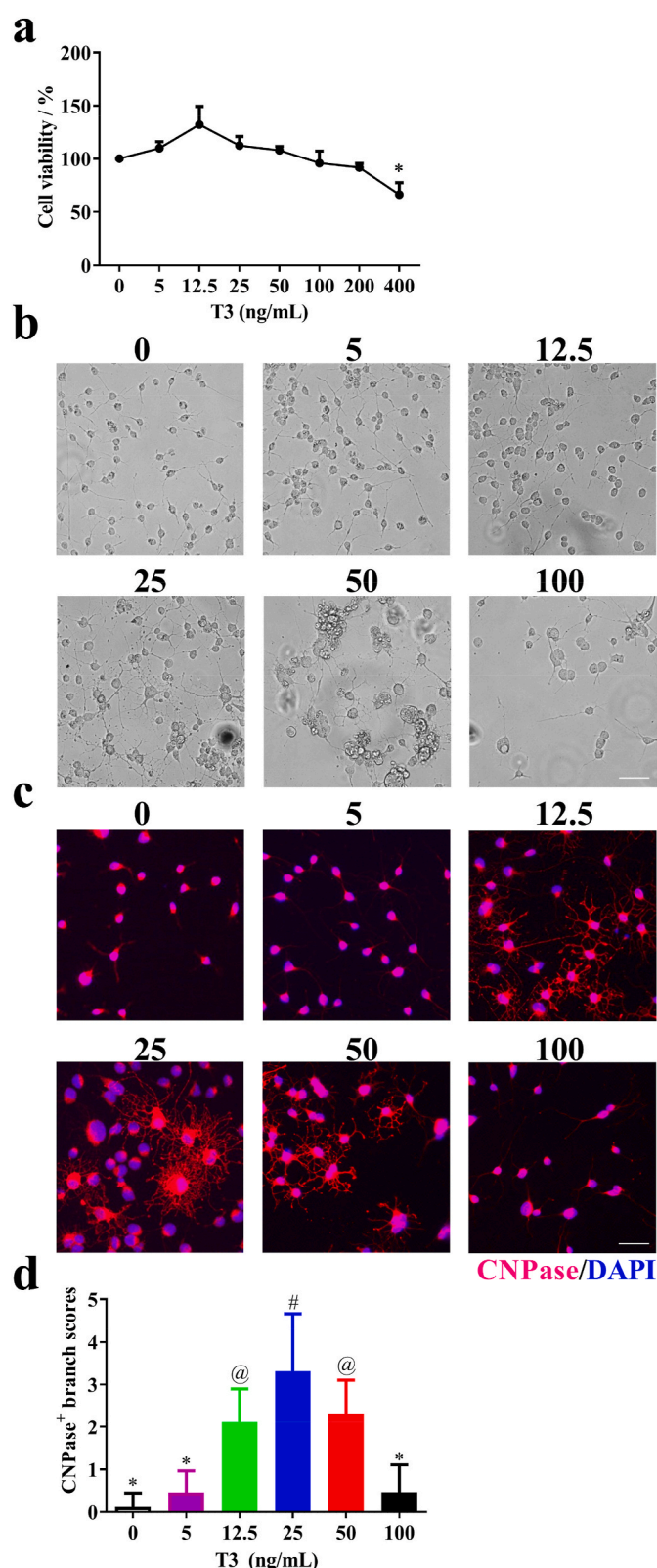


Fig. 1. Effect of T3 exposure on OPC differentiation *in vitro*. (a) Cell viability of T3 treatments. (b, c) OPCs were cultured with different concentrations of T3 under the OPC differentiation condition for 12 days and observed by microscope. (d) Quantitative analysis was performed to calculate the branch score of differentiated OLGs. Data are means \pm SD ($n = 5$ each group). Scale bar = 50 μm . Groups with different symbols are significantly different as determined by one-way ANOVA (* $p < 0.05$). Data are representative of three independent experiments.

standards, and treatment process all followed our previous studies [19]. Clinical scores were calculated blindly by two researchers daily according to a 0–5 scale as follows: 0.5, stiff tail; 1, limp tail; 1.5, limp tail and waddle with tail tonic; 2, partial paralysis of limb; 2.5, partial paralysis of limb with ataxia; 3, full paralysis of two hind limbs; 4, moribund; 5, death [4]. T3 was purchased from Sigma (Millipore Massachusetts, USA) and prepared in NaOH at 10 mg/ml for stock. EVPs, T3 (10 $\mu\text{g}/\text{kg}$) or EVPs + T3 (10 $\mu\text{g}/\text{kg}$) were injected intravenously (i.v.) every 3 days starting at the peak of disease.

2.9. Immunohistochemistry

Mice were sacrificed at day 30 post-immunization (p.i.). Tissues of the brain and spinal cords were fixed in 4% paraformaldehyde for 24 h and cut into 5 μm sections. Slides were stained with hematoxylin and eosin (H&E) or Luxol fast blue (LFB) to access the infiltration of inflammatory cells or myelin damage, respectively. Methods and criteria were referred to a previous study [20]. Fixation tissues were embedded in an optimum cutting temperature (OCT) compound (Tissue-Tek, Japan) and then sectioned coronally into 8 μm pieces. Slides were stained with specified primary and secondary antibodies. Images were recorded by a Nikon Eclipse Ci-s microscope (Tokyo, Japan) and a confocal microscope (Leica, Wetzlar, Germany).

2.10. Immunohistochemical analysis

Quantitative image analysis was performed using ImageJ (NIH) and Image-Pro (Media Cybernetics). To quantify MBP expression, the pixel intensity of immunofluorescence was measured. All slides were immunostained with MBP antibodies, and all digital images were acquired using the same exposure parameters. To quantify PDGFR⁺, NeuN⁺, APC⁺, O4⁺, or GFAP⁺ cells within the slices, 5–10 digital photographs were taken using the same exposure parameters from each section. The cell counter of Image-Pro software (Media Cybernetics) was used to count cells, and mean numbers were used for analysis.

2.11. Electron microscopy

EVs and EVPs were resuspended with PBS and used for transmission electron microscopy (TEM) images. Twenty microliters of EVs and EVPs were added to the carbon film copper grid for 10 min separately. One percent uranyl acetate was stained for 10 min at room temperature. Then, distilled water was used to clean the copper grid. After the copper grid dried in the air, images were observed using a TEM microscope (JEOL, Tokyo, Japan).

Lumbar spinal cords were fixed, and the lesion site of the dorsal spinal cord was taken for electron microscopy (Supplementary Fig. 1). It was then analyzed by TEM for assessing de/remyelination. Remyelinated axons were defined by an abnormally thin myelin sheath, which is considered the most reliable manner to identify remyelination. At least 50 myelinated axons on the figures were measured for each mouse. The g-ratio was measured by the size ratio between the diameter of the axon and the total fiber.

2.12. Nanoparticle tracking analysis (NTA)

EVs and EVPs were diluted in filtered (pore size = 100 nm) PBS, and the samples were tested by ZetaView PMX 110 (Particle Metrix, Meerbusch, Germany) previously by washing with PBS three times. The results of the mean size, size distribution, and particle amounts were acquired and analyzed with ZetaView 8.05.10.

2.13. Loading therapeutic cargo

To load the EVPs with T3, 1×10^8 particles of purified EVPs and 0.2 μg of T3 per mouse were gently mixed in 200 μl of PBS. The mixture was

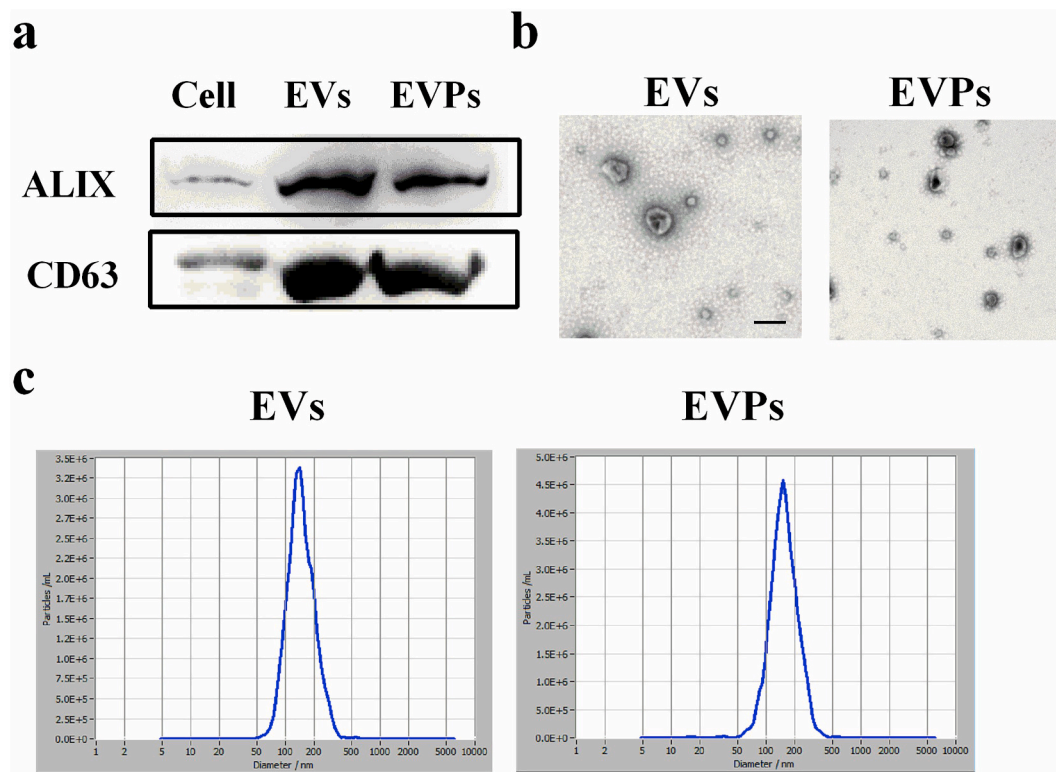


Fig. 2. Characterization of EVs and EVPs. (a) Western blot analysis of EVs and EVPs from NSCs for EV markers (ALIX and CD63). (b) Representative TEM images of EVs and EVPs. Arrows indicate typical EVs. Scale bar = 200 nm. (c) Size distribution of EVPs based on ZetaView PMX detection. One representative of three independent experiments is shown.

sonicated by an ultrasonic cell pulverizer (Scintez, Ningbo, China). Then the mixture was incubated for 0.5–1 h at 37 °C. Free T3 was eliminated by PD SpinTrap G-25 (GE Healthcare, Pittsburgh, USA). Mice were also treated with the filtrate. In addition, the EliKine Triiodothyronine (T3) ELISA Kit (Abbkine, China) was used to test the loading efficiency of T3 in EVPs.

2.14. IVIS imaging

EAE was induced at day 15 d.p.i., and mice were i.v. injected with EVs and EVPs marked with DiR lipophilic dye (Thermo Fisher Scientific) separately. In brief, following the manufacturer's instructions, EVs/EVPs were incubated with DiR at 37 °C for half an hour, and then the free DiR was cleared by a PD SpinTrap G-25 column (GE Healthcare). The same volume of DiR was used as the control in subsequent experiments. Mice were i.v. administered DiR-labeled EVs/EVPs and free DiR, and images were acquired using IVIS (PerkinElmer, Waltham, USA) after 24 h. Mice were sedated with isoflurane and live imaged using 10 s exposures and an ICG filter at 745 nm excitation. After each live imaging, the mouse organs were isolated and imaged using 10 s exposures (ICG filter at 745 nm excitation). Fluorescence for each mouse and organ image was quantified using Live Imaging Software in IVIS.

2.15. RNA extraction and real-time PCR

The total RNA of tissues was extracted using the RNeasy Pure Tissue Kit (Qiagen Biotech, Beijing, China). Reverse transcription was conducted using the PrimeScript RT Master Mix (Takara Bio, Dalian, China). Real-time PCR was performed using the ChamQTM SYBR qPCR Master Mix (Takara) and Roche Molecular Biochemicals LightCycler Software version 3.5 (Roche, Nutley, USA). Primer sets for murine genes are listed in [Supplementary Table 2](#).

2.16. Western blot analysis

EVs and EVPs were lysed by RIPA buffer (Solarbio, China, Beijing), and protease inhibitor phenylmethanesulfonyl fluoride was added. Protein concentration was measured by a BCA kit (Zoman Biotechnology, Beijing, China), and the same operation was performed on the NSCs to extract protein. The extracted protein was mixed with loading buffer to run polyacrylamide gel electrophoresis. The gel was incubated with a PVDF membrane to transfer the protein. Then, anti-CD63 (System Bioscience) and anti-Alix (Abcam, Cambridge, UK) antibodies were used in the experiment. Subsequently, the membranes were observed in a chemiluminescence analysis system (Tanon, Shanghai, China).

2.17. Statistics

Data were analyzed using GraphPad Prism 6.0 software (GraphPad, La Jolla, USA), and data are presented as the mean \pm SD. Significant differences in comparing multiple groups were analyzed by one-way ANOVA. All other statistical comparisons were made using the *t*-test. $P < 0.05$ was considered statistically significant.

3. Results

3.1. T3 promotes OPC differentiation at low concentration

T3 treatment of OPCs induces their differentiation into OLGs. T3 also invokes morphological expansion of OLGs, as indicated by the marked enhancement in the range of OLG branches. However, high doses of T3 result in cytotoxicity and are of concern [21,22]. To investigate the effect of T3 on OPCs, we characterized its effect on the viability of OPCs *in vitro*. To determine the optimal dosage of T3 for OPCs, we determined the cell viability under different T3 concentrations. Above the concentration of 25 μ M, T3 gradually reduced the cell viability of OPCs, and it

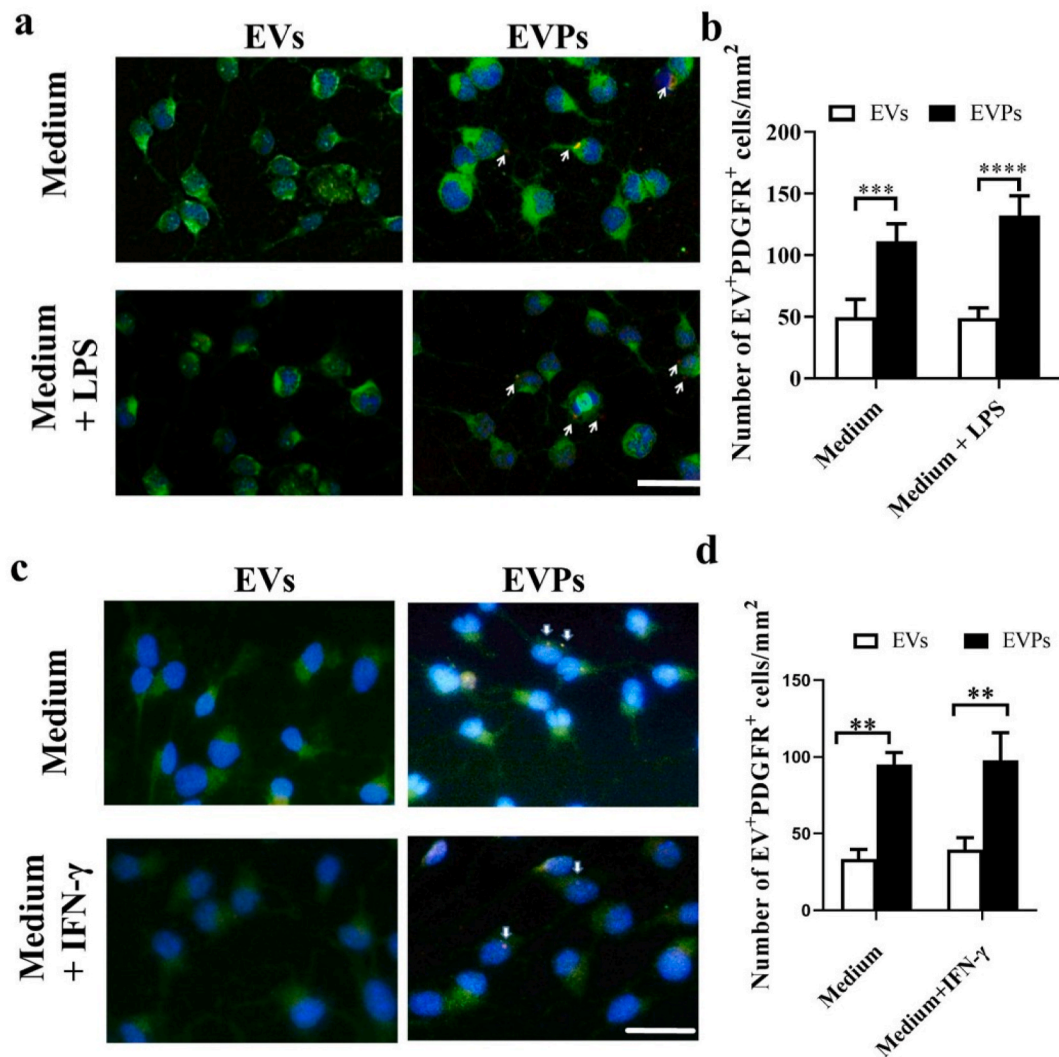


Fig. 3. The tropism of EVPs to primary OPCs *in vitro*. (a) EVs and EVPs were purified from NSCs labeled with ExoGlow membrane EV labeling kit for 2 h. Dye-labeled EVPs showed significantly higher tropism compared with EVs. (b) Numbers represent the quantification of OPCs that have interacted with dye-labeled EVs (dye positive OPCs). Scale bar = 50 μ m. Data are shown as mean values \pm SD ($n = 10$ for each group). T-tests were used to determine p values (** $p < 0.01$, *** $p < 0.001$, **** $p < 0.0001$). One representative of three independent experiments is shown.

decreased significantly when the concentration reached 400 μ M (Fig. 1a). We also found that the vehicle used for T3 treatment did not affect cell viability (Supplementary Fig. 2).

To determine the optimal dosage for OPCs differentiation, various concentrations of T3 were tested under the OPC differentiation condition. After 12 days, OPCs efficiently differentiated into OLGs at the concentrations of 12.5, 25, and 50 μ M, as observed under a light microscope and stained by CNPase antibody (Fig. 1b and c). OLGs showed more extended branches with complex web morphology at 25 μ M compared to other concentrations (Fig. 1d). These results confirmed that high doses of T3 have a negative effect on the proliferation and differentiation of OPCs, and the optimal dosage is 25 μ M, which significantly converts OPCs to OLGs.

3.2. PDGFR α serves as a potential target for drug delivery

As a demyelination disease, MS is difficult to cure. One of the reasons is that a large number of OPCs accumulate in the lesion area but cannot differentiate into OLGs [23]. Therefore, transporting therapeutic drugs to an effective site may ameliorate the disease development. Here, we tested the expression level of PDGFR α in the brain and spinal cord of EAE and naïve mice. The results indicated that the expression of PDGFR α was

significantly enhanced in both the brain and spinal cord of EAE mice, indicating that PDGFR α may serve as a potential target for drug delivery (Supplementary Fig. 3a). To achieve effective drug delivery to the lesion area, the Lenti-XStamp technology to overexpress the ligand of PDGFR α was used in this study. Briefly, the technology utilizes the localization of MFG-E8 on EVs and fuses the C1C2 domain of the protein gene (XStamp domain) with the PDGFA, a ligand of PDGFR α , and a 5' signal peptide is added before PDGFA. The “exposed ligand” part is anchored on the surface of EVs and leads them to the desired area. The schematic vector of XStamp-PDGFA is shown in Supplementary Fig. 3b.

3.3. Production and characterization of NSC-derived EV-PDGFA

NSCs are highly pluripotent cells with the capacity for self-renewal and possess the multidirectional potential for differentiation into neurons, astrocytes, and OLGs [24]. Additionally, NSCs have trophic function and strong proliferation capacity [4]. These beneficial characteristics enable NSCs to serve as a repository for the isolation of EVs. Here, the EVs were purified from the cell culture supernatants of XStamp-PDGFA and empty XStamp transfected NSCs by ultracentrifugation, called EVPs and EVs, respectively. EVPs and EVs were obtained as described in the Materials and Methods and were detected by Western

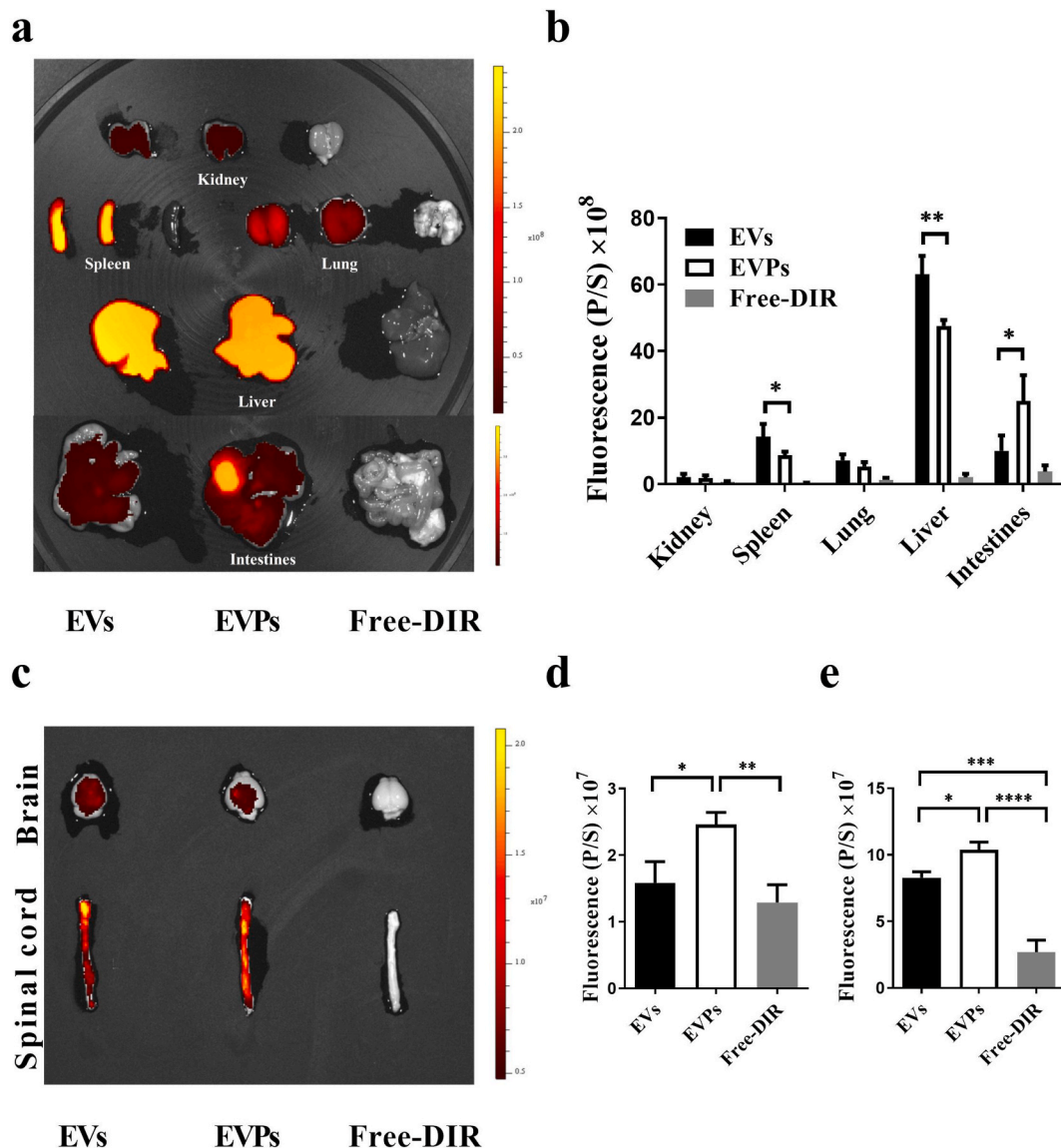


Fig. 4. Biodistribution of EVs/EVPs in vivo. (a) The peak of EAE mice were injected with DiR-labeled EVs/EVPs and free-DiR (control). Representative IVIS images of peripheral tissue (spleen, lung, kidney, intestines, and liver) at 24 h post-injection of DiR-labeled EVs/EVPs and free-DiR. (b) Quantification of fluorescent signals in peripheral tissue (spleen, lung, kidney, intestines, and liver) from Fig. 4a. (c) Representative IVIS images of the brain and spinal cords 24 h post-injection of DiR-labeled EVs/EVPs and free-DiR. (d) Quantification of the fluorescent signal in the brain at 24 h post-injection of DiR-labeled EVs/EVPs and free-DiR. (e) Quantification of the fluorescent signal in the spinal cords at 24 h post-injection of DiR-labeled EVs/EVPs and free-DiR. (n = 3, *p < 0.05; **p < 0.01, ***p < 0.001, ****p < 0.0001). One-way ANOVA was used to determine p values. One representative of three independent experiments is shown.

blot, TEM, and NTA. Western blot results verified that EVs and EVPs both expressed EV-specific markers CD63 and Alix (Fig. 2a) and indicated that EVs were purified from NSCs. TEM imaging demonstrated that both EVs and EVPs displayed a representative pattern (Fig. 2b). NTA determined the average diameter and particle concentrations from EVs and EVPs, respectively (Fig. 2c) and did not show any significant difference between these two groups. These results suggest that EVs and EVPs are accurately and highly efficiently separated from NSC culture medium.

3.4. EVPs enhance targeting delivery efficiency in vitro

To evaluate whether EVPs are able to increase the OPC targeting ability in vitro compared with EVs, EVPs and EVs were both incubated with ExoGlow-Membrane (System Biosciences) and cultured with OPCs. LPS (100 ng/ml) and IFN- γ (10 ng/ml) were also added to cells to simulate *in vivo* inflammation conditions. Immunofluorescence staining

showed that PDGFR⁺ OPCs were more inclined toward endocytosis EVPs but not EVs (Fig. 3a–d). These results suggest that choosing PDGFA (ligand of PDGFR) as a target ligand for PDGFR⁺ OPC cells is appropriate for the presented experiment in the EAE model, as well as for further demyelination disease application.

3.5. EVPs enhance targeting delivery efficiency in vivo

To verify the targeting ability of the EVPs in the animal model, the biodistribution was tested by IVIS. EVs or EVPs labeled with DiR were i. v. injected into the EAE mice in the same amounts. Twenty-four hours later, mice were sacrificed, and the tissues were dissected for the IVIS data process. Not surprisingly, about 40%–60% of the injected dose could be detected in the liver and 10% in the lung [25]. We also found EVs and EVPs abundantly distributed in the spleen and intestine. In addition, fewer EVPs were observed in the spleen and liver compared to EVs (Fig. 4a and b). Correspondingly, the EVP-treated group showed

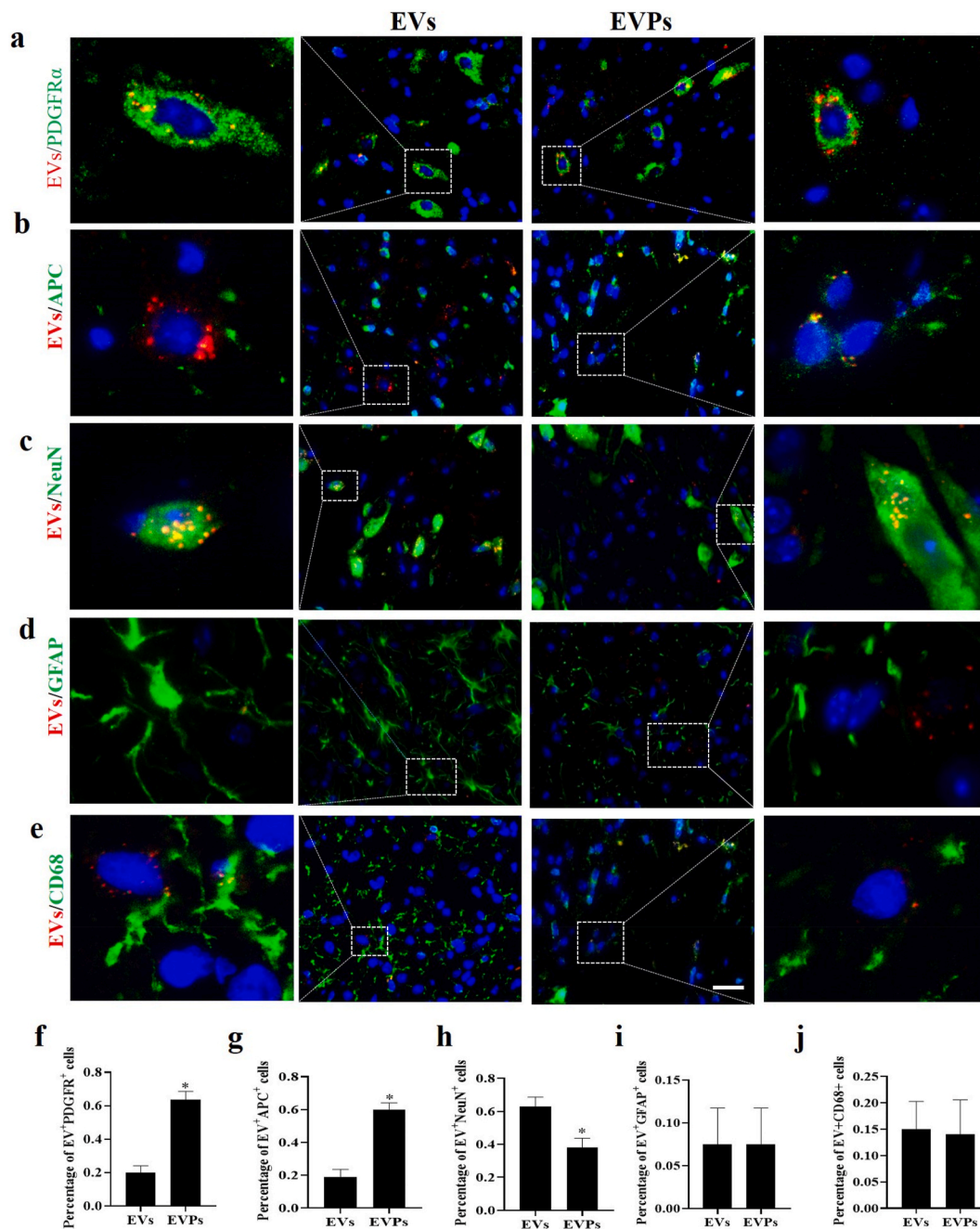


Fig. 5. Redirection of targeting EVPs *in vivo* and quantitative analysis of modification efficiency on EVPs. For *in vivo* distribution, EVs (1×10^8 particles) were labeled with ExoGlow membrane EV labeling kit and i.v. injected into the EAE mice (17 d.p.i.). After 5 days, mice were sacrificed, and spinal cords were harvested for fluorescent microscopy imaging. (a,b,c,d,e) Fluorescent microscopy images for the internalization of label EVs into recipient cells. Arrow indicated EVs intake by positive cells, whereas asterisk indicated EVs intake by negative cells. (f,g,h,i,j) Cell distribution and quantitative positive cell numbers were analyzed in different types. Scale bar = 100 μ m. T-tests were used to determine p values ($*p < 0.05$). One representative of three independent experiments is shown.

significantly higher fluorescence intensity in the brain and spinal cord compared with EV-treated mice (Fig. 4c and d). These findings indicated that EVPs may have the ability to target lesions in the spinal cord, which, in accordance with our results, shows that PDGFR α is highly expressed in demyelinated areas.

Further, to evaluate the uptake efficiency by various CNS cell types *in vivo*, EAE mice were i.v. injected with EVPs or EVs labeled with ExoGlow-Membrane (1×10^8 particles/mouse) on day 17 p.i. (disease peak). Five days later, mice were sacrificed, and the spinal cords were harvested for fluorescence detection. The data indicated that EVs had a higher delivery efficiency to neurons, but it was lower in oligodendrocyte lineages (Fig. 5c, h). However, EVPs had an enhanced ability to

target oligodendrocyte lineage cells, and the data indicated that more red fluorescence signals were taken up by PDGFR α^+ and APC $^+$ (mature oligodendrocyte) cells (Fig. 5a, b, f, g). Meanwhile, we did not observe a significant difference between EVs and EVPs in astrocytes or microglia (Fig. 5d, e, i, j). These results suggested that EVPs had significantly upgraded target efficiency for oligodendrocyte lineage cells but not for other neural cells. Because the expression level of PDGFR is significantly elevated in the spinal cord of EAE mice, these data confirmed the importance of EVP surface protein PDGFA in assisting EVP uptake. Taken together, these findings showed that EVPs not only improve delivery efficiency to lesions of the spinal cord but also act an accurate anchor to PDGFR α^+ cells.

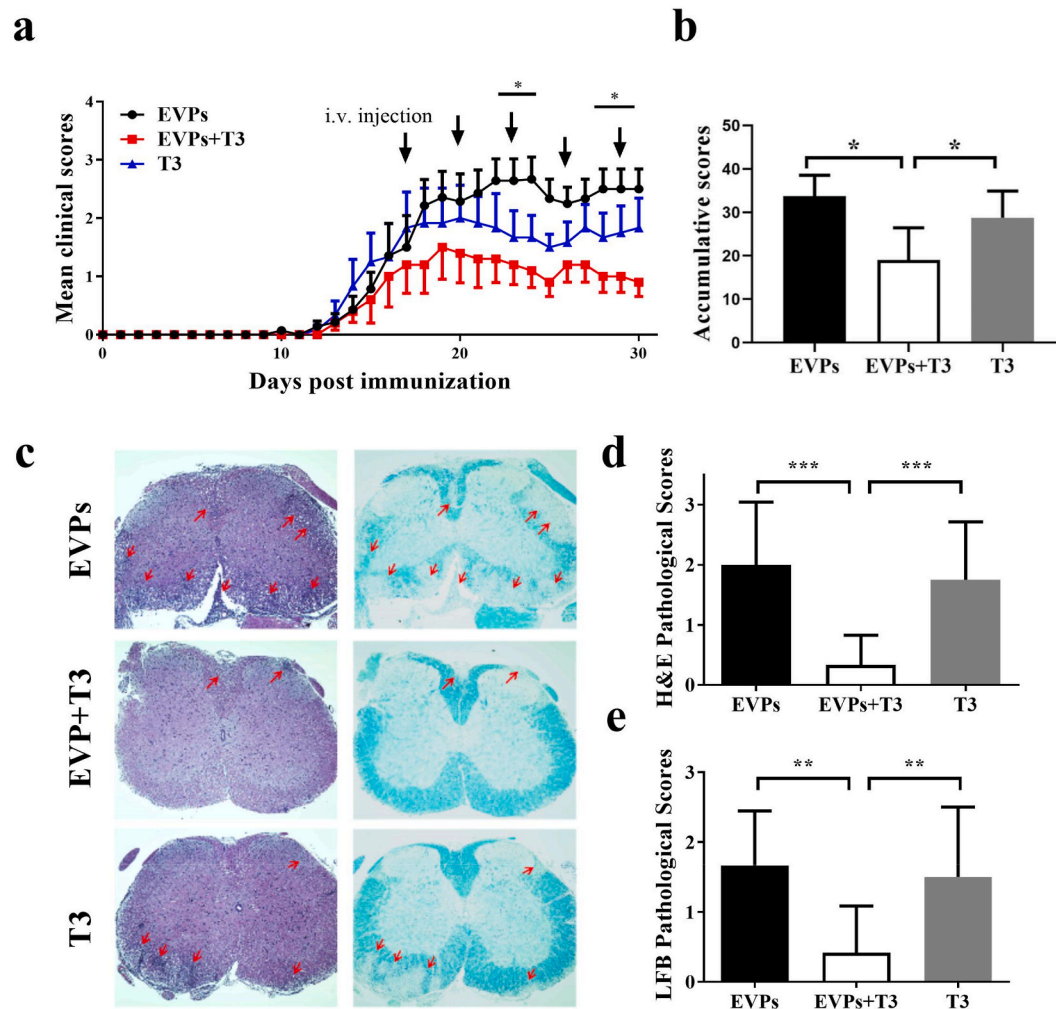


Fig. 6. EVPs + T3 alleviated disease development in the EAE model. C57BL/6 mice were injected i.v. with EVPs, T3 (5.19 $\mu\text{g}/\text{kg}$) or EVPs + T3 (10 $\mu\text{g}/\text{kg}$) every 3 days and starting at day 17 p.i.. (a) Clinical score was recorded daily following a 0–5 scale. The symbols (stars, *) refer to the difference between EVPs and EVPs + T3. (b) The cumulative clinical score of each mouse was calculated by summing up the scores of the mouse from day 0 to day 30 p.i.. (c) Mice were sacrificed at day 30 p.i. and spinal cords were harvested. Sections at lumbar level (L3) stained by H&E and LFB (scale bar = 500 μm), and pathology scores of inflammation (d) and percentage of demyelination area (e) evaluated. Data are mean \pm SD ($n = 5$ for each group). * $p < 0.05$, ** $p < 0.01$ and *** $p < 0.001$, determined by two-way ANOVA (a), or one-way ANOVA. (b, d, e). Data are representative of three independent experiments.

3.6. EVPs + T3 treatment alleviates disease development of EAE

To test the therapeutic effect of EVPs on demyelinated disease development, we first determined the EVP loading T3 efficiency to be 51.90% through ELISA (Supplementary Fig. 4a). Then the EAE mice were i.v. injected with 1×10^8 EVP particles carrying T3 ($\approx 5.19 \mu\text{g}/\text{kg}$) or non-loaded EVPs or T3 (10 $\mu\text{g}/\text{kg}$) alone every three days, starting at day 17 p.i. As indirect evidence of the presence of EVP-T3 in the CNS, we can see PDGFR α^+ THR α^+ in the demyelination area (Supplementary Figs. 4b and c). The EVPs-treated group of mice showed similar disease development trends to the PBS-treated group. Therefore, the PBS-treated group was omitted in the follow-up experiments. The EAE mice demonstrated the first sign of disease on day 11 p.i. The treatment of EVPs + T3 and T3 alone started on day 17 p.i. At the treatment period, the T3-treated group showed ameliorated disease development compared with the EVPs group, but did not show any significant difference in the clinical score statistic. This is likely due to the lower dosage of T3, which made it hard to reach the lesion area. Compared with T3-treated mice, the clinical score of EVPs + T3 showed an obvious decrease from day 23 p.i. Further, EVPs + T3-treated mice showed significant disease amelioration compared with EVP-treated mice, suggesting that the therapeutic potential of EVPs + T3 was considerably

higher than that of the other two groups (Fig. 6a). Then, we assessed pathological variation by histological analysis in lumbar spinal cords to detect CNS inflammatory infiltration and demyelination at day 30 p.i. Consistent with the clinical score, EVP-treated mice displayed severe EAE histological changes, while only a few infiltrating inflammatory cells present in the spinal cord white matter of the EVPs + T3-treated mice (Fig. 6b–d). To characterize possible blockage of demyelination or remyelination, EAE mice were treated with EVPs, EVPs + T3, or T3 starting on day 17 p.i., and the lumbar spinal cords were harvested on day 30 p.i. for Luxol fast blue (LFB) staining. As shown in Fig. 6c and e, EVP-treated mice demonstrated a progression of demyelination. Treatment with EVPs + T3 blocked this progression and could induce remyelination, as shown by the obvious myelin staining in the white matter area. Therefore, EVPs + T3 could extensively hinder demyelination or markedly induce remyelination compared with EVP or T3 treatment alone.

3.7. EVPs + T3 treatment increase the numbers of OLGs and block demyelination

Previous studies showed that OPCs aggregate to the lesion area but cannot differentiate due to the harsh environment [4]. Here, we showed

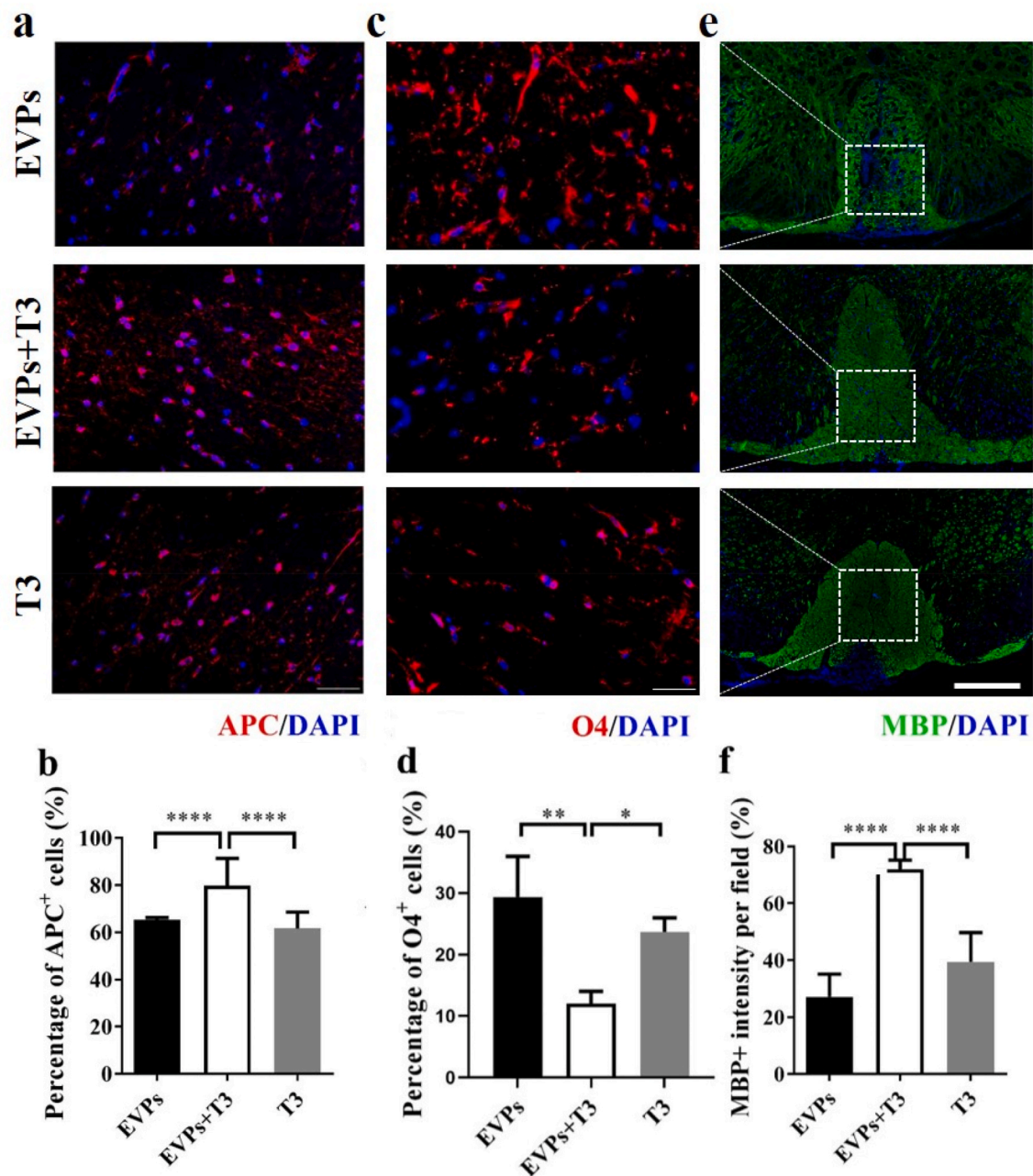


Fig. 7. EVPs + T3 treatment increased the numbers of OLGs and blockade demyelination. Mice described in Fig. 7a were sacrificed, and spinal cords were harvested at day 30 p.i. (a) Representative image of APC staining (mature OLG marker) counterstained with the nuclear dye DAPI (blue). (b) Percentage of APC⁺ cells. (c) Representative image of O4 staining (OPC marker) counterstained with the nuclear dye DAPI (blue). (d) Percentage of O4⁺ cells. (e) Representative image of MBP staining (myelin marker) counterstained with the nuclear dye DAPI (blue). (f) Quantification of MBP intensity. Scale bar = 50 μ m (a,c) and 100 μ m (e). Data are mean \pm SD, n = 5 for each group. *p < 0.05, **p < 0.01 and ****p < 0.0001, determined by one-way ANOVA comparison with Tukey's multiple comparison test.

the EVPs- and T3-treated groups also assembled abundant O4⁺ OPCs in the demyelination area. The number of APC⁺ mature oligodendrocyte significantly increased in the EVPs + T3-treated group compared with the EVPs- and T3-treated groups (Fig. 7a and b). Meanwhile, the EVPs + T3 treatment group showed fewer OPCs in the white matter area (Fig. 7c and d). Consistent with the growing APC⁺ oligodendrocyte numbers, the myelin staining area from the EVPs + T3-treated group showed higher MBP intensity compared with the other two groups (Fig. 7e and f). These results indicated that the myelin might contribute by those newly formed oligodendrocytes.

3.8. EVPs + T3 promote remyelination of demyelinated axons in the spinal cord

To further demonstrate that this therapeutic effect was due to the T3 carried by EVPs that achieved the remyelination, an ultrastructural electron microscope was used to detect the g-ratio as well as myelinated axons (Fig. 8a–d). Consistent with the results observed by immunohistochemistry, a thicker myelin sheath was found in the EVPs + T3-treated group compared with the other two groups. Although T3 treatment showed some signs of myelin regeneration, it was insignificant compared to EVPs + T3 treatment. The therapeutic effect is also manifested in the average g-ratio and percentage of myelinated axons (Fig. 8c and d). These results clearly demonstrated that EVPs + T3

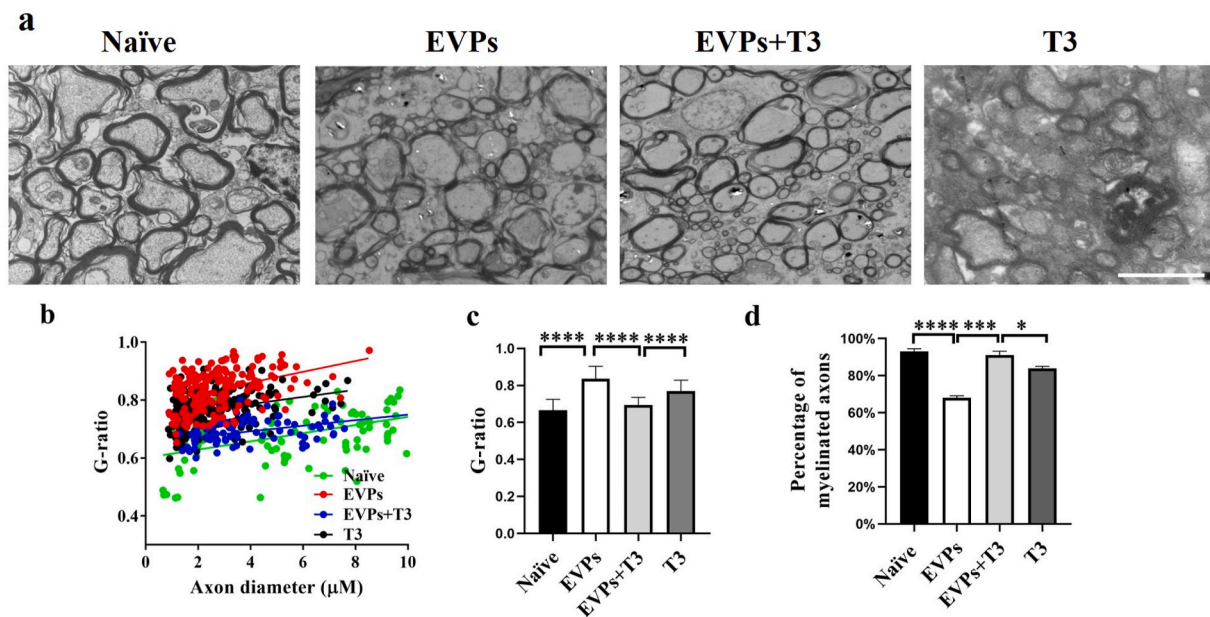


Fig. 8. EVPs + T3 treatment promoted myelination in the CNS. (a) Representative electron micrographs of transverse lumbar section of the ventral region. (b) Scatter plot of g -ratio of lesion axons. (c) Mean g -ratio (axon diameter divided by the entire myelinated fiber diameter) was determined using Image-Pro Plus software. (d) Quantification of the percentage of myelinated axons among total axons as shown. Scale bar = 20 μm . Data are mean \pm SD ($n = 100$ calculated from three mice per group). T-tests were used to determine p values (* $p < 0.05$, *** $p < 0.001$ and **** $p < 0.0001$). One representative of three independent experiments is shown.

significantly accelerated myelin regeneration compared with T3 treatment alone.

4. Discussion

Herein, we validated our primary hypothesis that NSC-derived EVs possess the natural ability to migrate to the CNS. However, an unexpected result showed that nearly 70% of NeuN⁺ neurons uptake EVs, which was confirmed by the immunofluorescence data. This means that EVs derived from natural NSCs cannot accurately deliver drugs to OPCs, which requires us to modify the EVs and increase the target efficiency. We supposed that a specific receptor gene would be highly expressed on the cell membrane during the proliferation/migration stage of OPCs. Therefore, we isolated the OPCs from naïve mice and EAE mice and used a microarray to determine the differential genes. Guided by this strategy, we expected to find the corresponding ligands armed with EVs enhancing the binding efficiency to OPC lineage cells. It is known that the PDGFR α is a marker protein of OPCs [21,23], which is also supported by our immunofluorescence and q-PCR data; this indicates that PDGFR α is a potential delivery target.

Unexpectedly, our data showed that APC⁺ mature OLGs take up a number of EVPs in the body. There may be two reasons for this phenomenon. On the one hand, more than 90% of PDGFR⁺ OPCs differentiate into mature oligodendrocytes. Therefore, EVPs may be taken up by OPCs before they differentiate into oligodendrocytes. On the other hand, newly formed oligodendrocytes also express moderate PDGFR, which helps EVP to enter oligodendrocytes.

Thyroid hormone (TH) regulates neural development, differentiation, and metabolism in mammals [22]. T3 is necessary for the production and maturation of OLGs and proper myelin formation [26]. It has been reported that administration of T3 increases myelin regeneration, axon protection, and nerve conduction preservation in several demyelinated animal models [27–29]. The promyelinating characteristics of T3 make it promising as a physiological molecule capable of treating demyelinating diseases such as MS. However, there exist several problems that need to be solved. One aspect to note is that T3 administration requires an appropriate dosage. Otherwise, a high

concentration of T3 may induce strong cytotoxicity [22]. This side effect was observed in our *in vitro* differentiation culture of primary OPCs (Fig. 1a). Another problem is that pro-inflammatory cytokines released from peripheral immune cells may suppress OLG differentiation. Cytokines such as TNF- α , IL-1 β , and IFN- γ could induce local hypothyroidism because these lipopolysaccharide-induced inflammations result in Dio2 dysregulation [5,30] and lead to downregulation of thyroid hormone receptor expression [31].

It is well known that TRs play an important role in remyelination. T3 exerts its action by binding TRs, a kind of nuclear receptor that migrates into the nucleus and mediates the expression of specific genes controlling the OPC cycle exit and regulating the expression of promyelinating genes [32]. However, a critical point is that the receptors are also expressed outside the CNS [33]. There is not yet any guideline for supraphysiological doses of T3 treatment in non-thyroid disease. Thus, the possibility of including T3 as adjuvant therapy in demyelinating disease during the acute inflammatory phase needs to be further considered. Emerging solutions for targeted drug delivery in the CNS based on biomaterials are vital here [31].

However, our ongoing studies have indicated that the macrophages residing in the liver and spleen can phagocytose a large number of EVs. This reduces the amount of EVPs + T3 entering the lesion site and reduces the therapeutic effect of T3. Moreover, some studies have found that EVs may be efficiently eliminated by the liver [34,35]. Therefore we need to find a new method to reduce the clearance efficiency of EVs by the liver and spleen. Furthermore, NSCs are found in the subventricular zone (SVZ) lining the lateral ventricles [36,37], making them difficult to obtain from patients. This will limit the availability of NSCs for use in clinical treatment. Mesenchymal stem cells (MSCs) are multipotent, nonhematopoietic cells with both immunomodulatory and regenerative properties [38]. Studies have shown that bone marrow mesenchymal stem cells (BM-MSCs) could reduce the inflammatory response, stimulate neuronal stem cell differentiation, and promote regeneration in damaged areas of the CNS [39–43]. Furthermore, several types of stem cells also possess therapeutic potential, such as autologous hematopoietic stem cells (aHSCs), human embryonic stem cells (hESCs), and induced pluripotent stem cells (iPSCs) [44].

In summary, our present study demonstrated that EVs derived from NSCs armed with PDGFA on their membrane surface exhibited significant target delivery ability to the demyelinated area in the CNS. The underlying biodistribution in the body was also investigated. Furthermore, we found that engineered EVPs loaded with T3 exerted significant remyelination effects in the lesion. Compared with EVP or T3 treatment alone, EVPs + T3 had obvious therapeutic effects, suppressing the disease development, promoting OPC differentiation, and protecting OLG survival, potentially solving the unmet medical need of treating demyelinating disease (Supplementary Fig. 5).

Author contributions

X.L. and Y.Z. conceived and designed the experiments. Y.X., J.T., W.W., Y.G., Y.G., S.S., and R.G. carried out the experiments. X.L., Y.Z., Y.X., and J.T. analyzed data and wrote the manuscript. X.L., Y.Z., L.W., and X.W. co-supervised the study and revised the paper. All authors read and approved the final manuscript.

Declaration of competing interest

This manuscript has not been published or presented elsewhere in part or in entirety and is not under consideration by another journal. We have read and understood your journal's policies, and we believe that neither the manuscript nor the study violates any of these. There are no conflicts of interest to declare.

Acknowledgments

This study was supported by the Chinese National Natural Science Foundation (Grant Nos.31970771, 82071396, 81771345), the Shaanxi Provincial Key R&D Foundation (Grant Nos. 2021ZDLSF03-09), the Science and Technology Projects of Ningxia Autonomous Region Key R&D Programs (2018BFG02017), the Natural Science Foundation of Ningxia Province, China (Grant Nos.2020AAC03397), the Fundamental Research Funds for the Central Universities (Grant Nos. GK202007022, GK202105002, TD2020039Y, 2020CSLZ009, 2021CSZL008).

Appendix A. Supplementary data

Supplementary data to this article can be found online at <https://doi.org/10.1016/j.bioactmat.2021.07.017>.

References

- [1] S.A. Goldman, N.J. Kuypers, How to make an oligodendrocyte, *Development (Camb.)* vol. 142 (2015) 3983–3995.
- [2] S.C. Starosom, J. Campo Garcia, T. Woelfle, S. Romero-Suarez, M. Olah, F. Watanabe, L. Cao, A. Yeste, J.J. Tupper, Chi3l3 induces oligodendrogenesis in an experimental model of autoimmune neuroinflammation 10 (1) (2019) 217.
- [3] M. Czepiel, E. Boddeke, S. Copray, Human oligodendrocytes in remyelination research, *Glia* 63 (4) (2015) 513–530.
- [4] X. Li, Y. Zhang, Y. Yan, B. Ciric, C.G. Ma, B. Gran, M. Curtis, A. Rostami, G. X. Zhang, Neural stem cells engineered to express three therapeutic factors mediate recovery from chronic stage CNS autoimmunity, *Mol. Ther. : J. Am. Soc. Gene Ther.* 24 (8) (2016) 1456–1469.
- [5] J.Y. Lee, S. Petratos, Thyroid hormone signaling in oligodendrocytes: from extracellular transport to intracellular signal, *Mol. Neurobiol.* 53 (9) (2016) 6568–6583.
- [6] S. Grade, L. Bernardino, J.O. Malva, Oligodendrogenesis from neural stem cells: perspectives for remyelinating strategies, *Int. J. Dev. Neurosci. : Off. J. Int. Soc. Dev. Neurosci.* 31 (7) (2013) 692–700.
- [7] A. Farsetti, B. Desvergne, P. Hallenbeck, J. Robbins, V.M. Nikodem, Characterization of myelin basic protein thyroid hormone response element and its function in the context of native and heterologous promoter, *J. Biol. Chem.* 267 (22) (1992) 15784–15788.
- [8] J. Bernal, A. Guadano-Ferraz, B. Morte, Thyroid hormone transporters—functions and clinical implications, *Nat. Rev. Endocrinol.* 11 (7) (2015) 406–417.
- [9] B. Gereben, A.M. Zavacki, S. Ribich, B.W. Kim, S.A. Huang, W.S. Simonides, A. Zeold, A.C. Bianco, Cellular and molecular basis of deiodinase-regulated thyroid hormone signaling, *Endocr. Rev.* 29 (7) (2008) 898–938.
- [10] G. Casella, F. Colombo, A. Finardi, H. Descamps, G. Ill-Raga, A. Spinelli, P. Podini, M. Bastoni, G. Martino, L. Muzio, R. Furlan, Extracellular vesicles containing IL-4 modulate neuroinflammation in a mouse model of multiple sclerosis, *Mol. Ther. : J. Am. Soc. Gene Ther.* 26 (9) (2018) 2107–2118.
- [11] Y. Tian, S. Li, J. Song, T. Ji, M. Zhu, G.J. Anderson, J. Wei, G. Nie, A doxorubicin delivery platform using engineered natural membrane vesicle exosomes for targeted tumor therapy, *Biomaterials* 35 (7) (2014) 2383–2390.
- [12] R. Shah, T. Patel, J.E. Freedman, Circulating extracellular vesicles in human disease, *N. Engl. J. Med.* 379 (10) (2018) 958–966.
- [13] T. Delong, T.A. Wiles, R.L. Baker, B. Bradley, G. Barbour, R. Reisdorph, M. Armstrong, R.L. Powell, N. Reisdorph, N. Kumar, C.M. Elso, M. DeNicola, R. Bottino, A.C. Powers, D.M. Harlan, S.C. Kent, S.I. Mannerling, K. Haskins, Pathogenic CD4 T cells in type 1 diabetes recognize epitopes formed by peptide fusion, *Science (New York, N.Y.)* 351 (6274) (2016) 711–714.
- [14] M. Garcia-Contreras, R.W. Brooks, L. Boccuzzi, P.D. Robbins, C. Ricordi, Exosomes as biomarkers and therapeutic tools for type 1 diabetes mellitus, *Eur. Rev. Med. Pharmacol. Sci.* 21 (12) (2017) 2940–2956.
- [15] R. van der Meel, M.H. Fens, P. Vader, W.W. van Solinge, O. Eniola-Adefeso, R. M. Schifferers, Extracellular vesicles as drug delivery systems: lessons from the liposome field, *J. Contr. Release : off. J. Controlled Release Soc.* 195 (2014) 72–85.
- [16] F. Geraci, P. Ragonese, M.M. Barreca, E. Aliotta, M.A. Mazzola, S. Realmuto, G. Vazzoler, G. Savettieri, G. Sconzo, G. Salemi, Differences in intercellular communication during clinical relapse and gadolinium-enhanced MRI in patients with relapsing remitting multiple sclerosis: a study of the composition of extracellular vesicles in cerebrospinal fluid, *Front. Cell. Neurosci.* 12 (2018) 418.
- [17] D. Rufino-Ramos, P.R. Albuquerque, V. Carmona, R. Perfeito, R.J. Nobre, L. Pereira de Almeida, Extracellular vesicles: novel promising delivery systems for therapy of brain diseases, *J. Contr. Release : off. J. Controlled Release Soc.* 262 (2017) 247–258.
- [18] Y. Zhang, X. Li, B. Ciric, C. Ma, B. Gran, A. Rostami, G. Zhang, Effect of fingolimod on neural stem cells: a novel mechanism and broadened application for neural repair, *Mol. Ther. : J. Am. Soc. Gene Ther.* 25 (2) (2017) 401–415.
- [19] L. Zhao, X. Li, Z.Q. Ye, F. Zhang, J.J. Han, T. Yang, Z.Z. Wang, Y. Zhang, Nutshell extracts of *xanthoceras sorbifolia*: A new potential source of bioactive phenolic compounds as a natural antioxidant and immunomodulator 66 (15) (2018) 3783–3792.
- [20] Y. Zhang, J.J. Han, X.Y. Liang, L. Zhao, F. Zhang, J. Rasouli, Z.Z. Wang, G. X. Zhang, X. Li, miR-23b suppresses leukocyte migration and pathogenesis of experimental autoimmune encephalomyelitis by targeting CCL7, molecular therapy, *J. Am. Soc. Gene Ther.* 26 (2) (2018) 582–592.
- [21] H.A. Abbaszadeh, T. Tiraihi, A.R. Delshad, M. Sagheddi Zadeh, T. Taheri, Bone marrow stromal cell transdifferentiation into oligodendrocyte-like cells using triiodothyronine as an inducer with expression of platelet-derived growth factor alpha as a maturity marker, *Iran. Biomed. J.* 17 (2) (2013) 62–70.
- [22] G.R. Kaka, T. Tiraihi, A. Delshad, J. Arabkheradmand, H. Kazemi, In vitro differentiation of bone marrow stromal cells into oligodendrocyte-like cells using triiodothyronine as inducer, *Int. J. Neurosci.* 122 (5) (2012) 237–247.
- [23] N.K. Koehler, M. Roebbert, K. Dehghani, M. Ballmaier, P. Claus, S. von Hoersten, M. Shing, P. Odin, J. Strehlau, F. Heidenreich, Up-regulation of platelet-derived growth factor by peripheral-blood leukocytes during experimental allergic encephalomyelitis, *J. Neurosci. Res.* 86 (2) (2008) 392–402.
- [24] X. Li, Y. Zhang, Y. Yan, B. Ciric, C.G. Ma, J. Chin, M. Curtis, A. Rostami, G. X. Zhang, LINGO-1-Fc-Transduced neural stem cells are effective therapy for chronic stage experimental autoimmune encephalomyelitis, *Mol. Neurobiol.* 54 (6) (2017) 4365–4378.
- [25] A. Pinheiro, A.M. Silva, J.H. Teixeira, R.M. Goncalves, M.I. Almeida, M.A. Barbosa, S.G. Santos, Extracellular vesicles: intelligent delivery strategies for therapeutic applications, *J. Contr. Release : off. J. Controlled Release Soc.* 289 (2018) 56–69.
- [26] M. Fernandez, A. Giuliani, S. Pironi, G. D'Intino, L. Giardino, L. Aloe, R. Levi-Montalcini, L. Calza, Thyroid hormone administration enhances remyelination in chronic demyelinating inflammatory disease, *Proc. Natl. Acad. Sci. U. S. A* 101 (46) (2004) 16363–16368.
- [27] P.G. Franco, L. Silvestroff, E.F. Soto, J.M. Pasquini, Thyroid hormones promote differentiation of oligodendrocyte progenitor cells and improve remyelination after cuprizone-induced demyelination, *Exp. Neurol.* 212 (2) (2008) 458–467.
- [28] J.C. Dugas, A. Ibrahim, B.A. Barres, The T3-induced gene KLF9 regulates oligodendrocyte differentiation and myelin regeneration, *Mol. Cell. Neurosci.* 50 (1) (2012) 45–57.
- [29] M.L. Dell'Acqua, L. Lorenzini, G. D'Intino, S. Sivilia, P. Pasqualetti, V. Panetta, M. Paradisi, M.M. Filippi, C. Baiguera, M. Pizzi, L. Giardino, P.M. Rossini, L. Calza, Functional and molecular evidence of myelin- and neuroprotection by thyroid hormone administration in experimental allergic encephalomyelitis, *Neuropathol. Appl. Neurobiol.* 38 (5) (2012) 454–470.
- [30] A. Boelen, J. Kwakkel, M. Platvoet-ter Schiphorst, A. Baur, J. Kohler, W. M. Wiersinga, Contribution of interleukin-12 to the pathogenesis of non-thyroidal illness, Hormone and metabolic research = Hormon- und Stoffwechselforschung = Hormones et metabolisme 36 (2) (2004) 101–106.
- [31] L. Calza, V.A. Baldassarro, M. Fernandez, A. Giuliani, L. Lorenzini, L. Giardino, Thyroid hormone and the white matter of the central nervous system: from development to repair, *Vitam. Horm.* 106 (2018) 253–281.
- [32] V.A. Baldassarro, W. Krezel, M. Fernandez, B. Schuhbauer, L. Giardino, L. Calza, The role of nuclear receptors in the differentiation of oligodendrocyte precursor cells derived from fetal and adult neural stem cells, *Stem Cell Res.* 37 (2019) 101443.
- [33] X.W. Alban Gaultier, Natacha Le Moan, Shinako Takimoto, Gatambwa Mukandala, Katerina Akassoglou, W. Marie Campana, Steven L. Gonias, Low-density

- lipoprotein receptor-related protein 1 is an essential receptor for myelin phagocytosis, *J. Cell Sci.* 122 (Pt 8) (2009) 1155–1162.
- [34] F. Willekens, J. Werre, J. Kruijt, B. Roerdinkholder-Stoelwinder, Y. Groenen-Döpp, A. van den Bos, G. Bosman, T. van Berkel, Liver Kupffer cells rapidly remove red blood cell-derived vesicles from the circulation by scavenger receptors, *Blood* 105 (5) (2005) 2141–2145.
- [35] R. van der Meel, M. Fens, P. Vader, W. van Solinge, O. Eniola-Adefeso, R. Schifflers, Extracellular vesicles as drug delivery systems: lessons from the liposome field, *J. Contr. Release : off. J. Controlled Release Soc.* 195 (2014) 72–85.
- [36] S. Weiss, C. Dunne, J. Hewson, C. Wohl, M. Wheatley, A. Peterson, B. Reynolds, Multipotent CNS stem cells are present in the adult mammalian spinal cord and ventricular neuroaxis, *J. Neurosci. : Off. J. Soc. Neurosci.* 16 (23) (1996) 7599–7609.
- [37] C. Morshead, B. Reynolds, C. Craig, M. McBurney, W. Staines, D. Morassutti, S. Weiss, D. van der Kooy, Neural stem cells in the adult mammalian forebrain: a relatively quiescent subpopulation of subependymal cells, *Neuron* 13 (5) (1994) 1071–1082.
- [38] M. Pittenger, A. Mackay, S. Beck, R. Jaiswal, R. Douglas, J. Mosca, M. Moorman, D. Simonetti, S. Craig, D. Marshak, Multilineage potential of adult human mesenchymal stem cells, *Science (New York, N.Y.)* 284 (5411) (1999) 143–147.
- [39] L. Bai, D. Lennon, V. Eaton, K. Maier, A. Caplan, S. Miller, R. Miller, Human bone marrow-derived mesenchymal stem cells induce Th2-polarized immune response and promote endogenous repair in animal models of multiple sclerosis, *Glia* 57 (11) (2009) 1192–1203.
- [40] E. Zappia, S. Casazza, E. Pedemonte, F. Benvenuto, I. Bonanni, E. Gerdoni, D. Giunti, A. Ceravolo, F. Cazzanti, F. Frassoni, G. Mancardi, A. Uccelli, Mesenchymal stem cells ameliorate experimental autoimmune encephalomyelitis inducing T-cell anergy, *Blood* 106 (5) (2005) 1755–1761.
- [41] J. Zhang, Y. Li, J. Chen, Y. Cui, M. Lu, S. Elias, J. Mitchell, L. Hammill, P. Vanguri, M. Chopp, Human bone marrow stromal cell treatment improves neurological functional recovery in EAE mice, *Exp. Neurol.* 195 (1) (2005) 16–26.
- [42] E. Gerdoni, B. Gallo, S. Casazza, S. Musio, I. Bonanni, E. Pedemonte, R. Mantegazza, F. Frassoni, G. Mancardi, R. Pedotti, A. Uccelli, Mesenchymal stem cells effectively modulate pathogenic immune response in experimental autoimmune encephalomyelitis, *Ann. Neurol.* 61 (3) (2007) 219–227.
- [43] K. Kemp, K. Hares, E. Mallam, K. Heesom, N. Scolding, A. Wilkins, Mesenchymal stem cell-secreted superoxide dismutase promotes cerebellar neuronal survival, *J. Neurochem.* 114 (6) (2010) 1569–1580.
- [44] F. Cuascut, G. Hutton, Stem cell-based therapies for multiple sclerosis: current perspectives, *Biomedicines* 7 (2) (2019) 26.